Development/Plasticity/Repair

Regulation of Gephyrin Cluster Size and Inhibitory Synaptic Currents on Renshaw Cells by Motor Axon Excitatory Inputs

David Gonzalez-Forero,[1,2] Angel M. Pastor,[2] Eric J. Geiman,[1] Beatriz Benítez-Temiño,[2] and Francisco J. Alvarez[1]

[1]Department of Anatomy and Physiology, Wright State University, Dayton, Ohio 45435, and [2]Departamento de Fisiología y Zoología, Facultad de Biología, Universidad de Sevilla, 41012-Sevilla, Spain

Renshaw cells receive a high density of inhibitory synapses characterized by large postsynaptic gephyrin clusters and mixed glycinergic/GABAergic inhibitory currents with large peak amplitudes and long decays. These properties appear adapted to increase inhibitory efficacy over Renshaw cells and mature postnatally by mechanisms that are unknown. We tested the hypothesis that heterosynaptic influences from excitatory motor axon inputs modulate the development of inhibitory synapses on Renshaw cells. Thus, tetanus (TeNT) and botulinum neurotoxin A (BoNT-A) were injected intramuscularly at postnatal day 5 (P5) to, respectively, elevate or reduce motor axon firing activity for ~2 weeks. After TeNT injections, the average gephyrin cluster areas on Renshaw cells increased by 18.4% at P15 and 28.4% at P20 and decreased after BoNT-A injections by 17.7% at P15 and 19.9% at P20. The average size differences resulted from changes in the proportions of small and large gephyrin clusters. Whole-cell recordings in P9–P15 Renshaw cells after P5 TeNT injections showed increases in the peak amplitude of glycinergic miniature postsynaptic currents (mPSCs) and the fast component of mixed (glycinergic/GABAergic) mPSCs compared with controls (60.9% and 78.9%, respectively). GABAergic mPSCs increased in peak amplitude to a smaller extent (45.8%). However, because of the comparatively longer decays of synaptic GABAergic currents, total current transfer changes after TeNT were similar for synaptic glycine and $GABA_A$ receptors (56 vs 48.9% increases, respectively). We concluded that motor axon excitatory synaptic activity modulates the development of inhibitory synapse properties on Renshaw cells, influencing recruitment of postsynaptic gephyrin and glycine receptors and, to lesser extent, $GABA_A$ receptors.

Key words: **motoneurons; development; spinal cord; botulinum toxin; tetanus toxin; $GABA_A$ receptor; glycine receptor; recurrent inhibition**

Introduction

Inhibitory synapses modulate excitatory inputs and shape neuronal firing. Therefore, inhibitory synaptic properties must be set according to excitatory input strengths and the firing activity of individual neurons. However, the inhibitory synapse properties that are influenced by local excitatory activity are poorly known. One important feature that affects inhibitory synaptic strength is receptor recruitment, and this in turn depends on postsynaptic density (PSD) structure (Nusser et al., 1997, 1998; Lim et al., 1999; Oleskevich et al., 1999). Indeed, we proposed that the size of postsynaptic clusters of gephyrin, a key scaffold protein of the inhibitory PSD (Triller et al., 1985; Kirsch et al., 1993; Kirsch and Betz, 1998), correlates with postsynaptic glycinergic current amplitudes (Lim et al., 1999; Van Zundert et al., 2004). In most neurons, larger gephyrin clusters occur in distal dendrites; however, Renshaw cells exhibit large proximal gephyrin clusters that colocalize glycine and $GABA_A$ receptors (Alvarez et al., 1997; Geiman et al., 2002a). Accordingly, glycine and GABAergic synaptic currents in Renshaw cells are larger than in other spinal interneurons (Gonzalez-Forero and Alvarez, 2005). The mechanisms that mature large gephyrin clusters and glycine/GABAergic currents in Renshaw cells are unknown.

Renshaw cells provide recurrent inhibition to motoneurons and modulate motoneuron recruitment, firing rate, and proprioceptive reflexes. The main excitatory input to Renshaw cells arises from cholinergic intraspinal recurrent collaterals of motor axons (Renshaw, 1946; Eccles et al., 1954; Alvarez et al., 1999) and results in vigorous long-lasting postsynaptic responses that evoke sustained firing with initial instantaneous frequencies of ~1500 Hz (Eccles et al., 1954). Even single action potentials propagating in individual motor axons induce high-frequency discharges in Renshaw cells in the anesthetized cat spinal cord (van Keulen, 1981). No other spinal interneuron shows similar synaptic responses to motor axons, and thus the specific presence of powerful inhibitory synapses on Renshaw cells suggests a relationship with the unique properties of their excitatory activity. Inhibitory synaptic properties on Renshaw cells develop during the first three postnatal weeks, in conjunction with the onset of locomotion and the maturation of ventral horn motor circuits (Geiman et al., 2000; Gonzalez-Forero and Alvarez, 2005). These observations led to the suggestion that inhibitory synapse development

Received July 21, 2003; revised Nov. 19, 2004; accepted Nov. 20, 2004.

This work was supported by National Science Foundation Grant 9984441 to F.J.A. and Ministerio de Ciencia y Tecnología–Fondo Europeo de Desarrollo Regional Grant BFI2003-01024 to A.M.P. D.G.-F. was supported by a postdoctoral fellowship from the Ministerio de Educación, Cultura y Deporte (Spain). We thank Drs. R. E. W. Fyffe, J. Stern, J. Dean, and S. P. Schneider for helpful suggestions during the performance of this work and Drs. T. Cope and B. Walmsley for helpful suggestions on previous versions of this manuscript.

Correspondence should be addressed to Dr. Francisco J. Alvarez, Department of Anatomy and Physiology, Wright State University, 3640 Colonel Glenn Highway, Dayton, OH 45435. E-mail: francisco.alvarez@wright.edu.

DOI:10.1523/JNEUROSCI.3725-04.2005

 0270-6474/05/250417-13$15.00/0

on Renshaw cells could be modulated by activity in their motor axon synaptic inputs (Geiman et al., 2000). To test this hypothesis, we developed an *in vivo* experimental model that permitted chronic alteration of motoneuron firing in neonates. We increased and reduced motor activity, respectively, with tetanus neurotoxin (TeNT) and botulinum neurotoxin serotype A (BoNT-A) during the period of maturation of inhibitory synapses on Renshaw cells [from postnatal day 5 (P5) to P20]. Then, we analyzed the resulting gephyrin clusters and inhibitory synaptic currents. We show that changes in motor axon activity significantly altered gephyrin clustering and glycine/$GABA_A$ synaptic currents. Thus, we concluded that activity at neighboring excitatory synapses influence the recruitment of inhibitory postsynaptic scaffolding proteins and receptors, suggesting a mechanism that helps match inhibitory synapses to local excitatory inputs.

Preliminary observations were presented in abstract form (Geiman et al., 2002b; Alvarez et al., 2004).

Materials and Methods

Toxin injections. Wistar rat pups of either sex received injections in the gastrocnemius with TeNT, BoNT-A, or vehicle (0.9% sterile saline) (both toxins were gifts from J. O. Dolly, Imperial College, London, UK). A second injection in the same muscle contained 1 μl of 1% Fast Blue and 1% Diamidino Yellow (EMS-Polyloy, GrossUmstadt, Germany) and was used to retrogradely label spinal cord sections containing the target motor pool.

Injections were made at P5 in the left gastrocnemius muscle under ether anesthesia after exposing the muscle via a small incision in the skin. The appropriate toxin doses or vehicle were delivered using 2 μl volume injections into the muscle belly. Then, the incisions were closed with Vet-seal (B. Braun Surgical, Emmenbrücke, Switzerland), and the animals were returned to their mothers after they fully recovered from anesthesia. Toxin effects, ankle tetanic extension after TeNT or ankle flaccid paralysis after BoNT-A injection, were monitored daily. To quantitatively analyze the time course of clostridial toxin action on motor output and the neuromuscular junction (NMJ), some animals were prepared for recording nerve activity or muscle tension at 6 hr after the injection or at 1, 2, 4, 6, 8, 10, 12, 14, and 16 d after the injections. For morphological analysis of gephyrin clusters in calbindin-immunoreactive (IR) Renshaw cells, treated animals were killed at P15 or P20. To analyze inhibitory currents (glycinergic and GABAergic) in Renshaw cells, we used a spinal cord slice preparation as described previously (Gonzalez-Forero and Alvarez, 2005). It is technically difficult to preserve intact motoneurons in this preparation beyond P15, and motoneuron stability seems important for obtaining good quality Renshaw cell recordings; thus, we targeted Renshaw cells of the ages P9–P15 to analyze inhibitory currents after toxin injections. Only animals showing clear toxin effects that started within the first 48 hr after injection were used in subsequent morphological or electrophysiological analyses.

Neonatal animals show decreased sensitivity to clostridial toxins (Pastor et al., 2003), therefore we first injected different doses of BoNT-A (from 5 to 100 ng/kg) in the gastrocnemius muscle of P5 neonatal rats and observed their efficiency at eliciting specific ipsilateral ankle paralysis with minimal effects on overall animal development. Survival rates, growth of the litters, and paralysis at the ankle or other joints ipsilateral and contralateral to the injection were noted for each dose. The final dose chosen was 30 ng/kg. At this dose, most animals survived the toxin injections and showed obvious flaccid paralysis restricted to the injected leg. Paralysis was noted by the lack of foot extension when touching the footpad and immobility of the ipsilateral foot when pinching the tail tip or grabbing the animal by the tail. In addition, paralyzed animals tended to drag the affected foot during locomotion. Animals that received injections of lower doses of toxin showed decreased levels of paralysis and faster recoveries. Higher doses led to increased mortality and the appearance of contralateral and systemic effects.

For TeNT, pups received injections of 25 ng/kg after testing initial doses ranging 15–50 ng/kg to find survival rates of >90% of the pups. Animals that received injections of 25 ng/kg showed specific ipsilateral tetanization of the ankle within 48 hr after injection (i.e., the affected foot is paralyzed in continuous extension). Tetanic extension lasted from 8 to 10 d and started to recover afterward.

Animals were inspected daily. Animals showing signs of distress were removed from the study. No significant differences in weight were observed between injected animals and littermates at the doses used for the study. In addition, animals were discarded if, after histological processing, few retrogradely labeled motoneurons were observed.

All animal procedures were performed according to National Institutes of Health guidelines approved by the Wright State University Laboratory Animal Use Committee and in accordance with the European Union (86/609/EU) and Spanish legislation (BOE 67/8509-12, 1988).

Recording of clostridial toxin actions on the NMJ. Measurements of NMJ function after TeNT or BoNT-A injections were obtained by comparing the force generated by the gastrocnemius muscle after direct stimulation of the muscle fibers or after nerve stimulation (indirect muscle fiber stimulation). Rat pups were decapitated, and the left leg was rapidly dissected out in cold Kreb's solution (in mM: 113 NaCl, 4.5 KCl, 1 $MgSO_4$, 2 $CaCl_2$, 11 glucose, 1 Na_2HPO_4, and 25 $NaHCO_3$). The calcaneal tendon of the gastrocnemius muscle and the calcaneous bone were detached from the ankle. Other ankle extensors were detached from the calcaneous bone and denervated so that they would not interfere with gastrocnemius contraction. The dissected leg was transferred to the recording bath, and the tibia was pinned down to a Sylgard base. The calcaneal tendon was secured to a strain gauge transducer (Dynamometer UF1; Pioden Controls) under isometric conditions and coupled to an amplifier (NL108; NeuroLog System; Digitimer, Welwyn Garden City, Hertfordshire, UK). A silver bipolar hook electrode was used for stimulation of the tibial nerve. One additional bipolar stimulating electrode was forked around the muscle belly. Forces generated by nerve stimulation were estimated by the average of three to six stimuli (15 V, 0.2 msec duration; delivered at 0.5 Hz). The force from direct muscle stimulation was averaged from the same number of stimuli (15 V, 2 msec duration; delivered at 0.5 Hz). Force transducer signals were digitized with a Micro1401 MK II analog-to-digital converter (5 kHz, 16 bit; CED, Cambridge, UK) and analyzed with Signal Averager (CED).

Recordings of motor nerve activity. Animals were anesthetized with ether (dose to effect) and surgically prepared for electroneurographic bilateral recordings of the tibial nerves. The tibial nerve was exposed and dissected free of connective tissue, and a bipolar hook electrode was shaped around the nerve to ensure gentle contact of both leads. Electrodes were made of 200 μm Teflon-insulated silver wire. The electrode location was insulated with Parafilm and bathed in mineral oil. The muscle and skin were sutured to hold the electrode in place, and the nerve was cut distal to the recording site. Then, the rat pups were allowed to slightly recover from anesthesia (there is little nerve activity when deeply anesthetized). The level of anesthesia kept the animal relaxed, and pups did not move during recordings. The electrocardiogram was audio monitored for fluctuations in heart rate during experiments. The rat pups were gently restrained in a small Perspex box gently cushioned with cotton so that the animal adopted a neutral resting position with the forelimbs extended. Lights were dimmed so not to startle the animal, and recordings were started. Simultaneous bursting nerve activity was evoked bilaterally by rubbing the tail with a glass probe. Electroneurographic activity was recorded AC-coupled in common mode rejection using a NL104 differential amplifier (Digitimer) and filtered from 10 Hz to 10 kHz plus a 50 Hz notch filter. The signal of control and treated nerves was half-wave rectified, and the area under the curve was measured in selected 1 sec periods of synchronic bursts of activity in control and treated sides for pairwise comparisons. The pups were euthanized at the end of the experiment.

Tissue preparation and immunocytochemical procedures. At P15 and P20, toxin-injected rat pups were fixed by perfusion with 4% paraformaldehyde in 0.1 M phosphate buffer (PB), pH 7.4, followed by 30 min postfixation in the same fixative, then washed and stored in 15% sucrose in 0.1 M PB until use. Forty-micrometer-thick sections from the L5 spinal cord segment were obtained on a freezing sliding microtome.

The sections were dual-immunolabeled for gephyrin (mouse mono-

clonal antibody; 1:100 in PBS containing 0.1% Triton X-100; Boehringer Mannheim, Indianapolis, IN) and calbindin (rabbit polyclonal antibody; 1:4000 dilution; Swant, Bellinzona, Switzerland). Renshaw cells were identified by their intense calbindin immunoreactivity (Antal et al., 1990; Ardvidsson et al., 1992; Sanna et al., 1993; Carr et al., 1998; Fallah and Clowry, 1999; Geiman et al., 2000; McDonough et al., 2001). Immunoreactive sites were visualized with donkey anti-rabbit, anti-mouse, or anti-goat IgGs coupled to cyanine 3 (Cy3) or FITC (Jackson ImmunoResearch, West Grove, PA).

Gephyrin cluster area analysis. Calbindin-IR Renshaw cells were chosen randomly for analysis at low magnification from sections containing ≥10 retrogradely labeled motoneurons. Gephyrin immunofluorescence was only imaged after the Renshaw cells to be used for analysis were selected. To guarantee that all somatic gephyrin clusters were imaged, only calbindin-immunolabeled Renshaw cells with the complete somata contained within the section were used. Then, gephyrin and calbindin immunofluorescence in Renshaw cells were simultaneously imaged at high magnification (60× oil immersion objective; numerical aperture, 1.4 digitally zoomed 3×; 1024 × 1024 pixel images; pixel size, 0.0064 μm^2) using an Olympus Fluoview FX confocal microscope. To obtain the highest quality cluster morphology, confocal settings were optimized for the best signal/noise ratio and to use the full dynamic range available (4095 intensity levels). Optical sections were obtained every 0.5 μm *z*-steps. This *z*-step size allowed image "oversampling" of most clusters, frequently identified in adjacent optical sections (focal optical depth of the objective, ~0.6–0.7 μm), and prevented the loss of the dimmer and smaller clusters, usually imaged in just one focal plane. Gephyrin clusters were analyzed in confocal image stacks of the whole-cell body using Image Pro Plus software (version 4.1; Media Cybernetics, Silver Spring, MD). Confocal images were analyzed one optical section at a time for all *en face* clusters present at the top and bottom surfaces (supplemental Fig. 1, available at www.jneurosci.org as supplemental material). The focal depth of our objective was more than enough to image the whole extent of *en face* clusters within the optical section. *En face* clusters were only measured in optical sections where they displayed the maximum immunofluorescence brightness. Clusters imaged through many optical sections were frequently not *en face* and lie on regions of high membrane curvature. These tangential clusters were excluded from the analysis given the difficulty of getting accurate size estimates from them. Measured clusters represent approximately one-third of all clusters on the cell bodies of individual neurons. This relatively high proportion of *en face* clusters results in part because of flattening of the neurons in the *z*-axis within the histological preparation. Renshaw cells were defined by their strong calbindin immunofluorescence. Individual gephyrin clusters in Renshaw cells were segmented automatically from the image by using a threshold level equal to 25–33% of the maximum brightness in each optical section. This value was empirically defined according to gephyrin immunofluorescence brightness in different animals such that thresholded clusters were traced just inside the fluorescence diffraction halo. This tracing perimeter was previously found to result in the most accurate measurements of cluster size and was comparable to electron microscopic observations (Geiman et al., 2000). Differences in cluster immunofluorescence brightness because of depth within the tissue were corrected by relating the thresholding criteria to the maximum brightness recorded in each optical section. Areas were measured for all *en face* gephyrin clusters found at the top and bottom surfaces of the neuron. We also recorded maximum and minimum diameters, integrated optical density, and immunofluorescence density. We did not analyze intensity values further because we observed a systematic decrease in brightness with tissue depth. Most of this decrease should be attributed to variable amounts of light dispersion induced by the tissue. These alterations in intensity did not affect area measurements (i.e., *en face* clusters sampled at each side of the cell showed no significant differences in average area). We previously showed that small changes in immunofluorescence intensity do not significantly change the apparent sizes of gephyrin clusters (Geiman et al., 2000). For cluster density measurements, all gephyrin clusters on Renshaw cell somata were counted and divided by the surface area of Renshaw cell somata. Surface areas were estimated by approximating the cell body to an ellipsoid of the same maximum and minimum diameters.

Whole-cell recordings of inhibitory currents. We recorded ventral horn interneurons from spinal cord slices obtained from P9–P15 animals that received injections of TeNT (25 ng/kg) at P5, as described above. Renshaw cell recordings were obtained as described previously (Gonzalez-Forero and Alvarez, 2005). Animals received injections of FITC-conjugated cholera toxin fragment B (CTb) (2.5% in saline) in the gastrocnemius muscle 2–5 d before electrophysiological recordings. Retrograde transport of CTb allowed visualization of the gastrocnemius motoneuron pool. Sections with large numbers of retrogradely labeled motoneurons were identified at low magnification (4×) using epifluorescence (Olympus BX 50WI microscope), and then small ventral interneurons (<20 μm diameter) were sampled in the "Renshaw cell region" using infrared differential interference contrast optics and high magnification (40×; water immersion). Recorded neurons were identified after recording as Renshaw cells using neuroanatomical histochemical criteria as described below.

Animals were anesthetized (50 mg/kg pentobarbital) and decapitated, and their spinal cords were removed quickly. Dissection was in ice-cold (<4°C) sucrose-modified artificial CSF (S-aCSF) bubbled with 95% O_2 and 5% CO_2. S-aCSF composition was as follows (in mM): 26 $NaHCO_3$, 10 glucose, 3 KCl, 1.25 NaH_2PO_4, 2 $MgCl_2$, 2.4 $CaCl_2$, and 218 sucrose. Transverse slices from the L4–L5 segments (300–400 μm thick) were cut using an OTS-4000 tissue slicer (Electron Microscopy Sciences, Fort Washington, PA). Slices were transferred to normal oxygenated aCSF (in which sucrose was removed and 130 mM NaCl and 2 mM $CaCl_2$ were added) and incubated for 1 hr at 36°C and then stabilized at room temperature (22–25°C) for at least 30 min before electrophysiological recordings. Finally, the slices were transferred into the recording chamber and perfused (at a rate of 4 ml/min) with oxygenated normal aCSF at room temperature. Patch electrodes (2–5 MΩ resistance) contained the following (in mM): 120 CsCl, 4 NaCl, 4 $MgCl_2$, 1 Cl_2Ca, 10 HEPES, 0.2 EGTA, 3 Mg-ATP, and 0.3 GTP-Tris. In all of the experiments, 0.4% neurobiotin (Vector Laboratories, Burlingame, CA) was added to the internal solution. Only recordings with access resistance between 5 and 20 MΩ were accepted for analysis. Access resistance was monitored continuously, and the recording was abandoned if it changed >15%. Junction potentials were corrected after inserting the pipette into the bath. Cells were voltage clamped at −75 mV. The reversal potential for chloride currents was close to 0 mV; thus, GABAergic and glycinergic currents were readily detected as inward currents well separated from baseline noise. Synaptic currents were recorded and low-pass bessel filtered at 5 kHz with a Axopatch 200B amplifier (Axon Instruments, Union City, CA). Data were digitized at 10 kHz and acquired using Axograph (version 4.6; Axon Instruments). For each cell, we obtained two to three segments of 5 min continuous recordings of pharmacologically isolated spontaneous synaptic currents of interest.

Miniature spontaneous synaptic currents of GABAergic and/or glycinergic origin (mPSCs) were isolated with tetrodotoxin (TTX) (1 μM; Alomone, Jerusalem, Israel), 6-cyano-7-nitroquinoxaline-2,3-dione (CNQX) (10 μM; Tocris, Bristol, UK), and D-tubocurarine chloride (30 or 10 μM; Sigma, St. Louis, MO) applied by bath perfusion. Glycinergic or GABAergic mPSCs were subsequently isolated by adding either bicuculline methiodide (10 μM; Sigma) or strychnine hydrochloride (0.25 μM; Sigma).

Off-line data analysis was performed using pClamp 9.0 and MiniAnalysis software (Synaptosoft). Events were detected by setting a detection threshold value of three times the root mean square noise. The detection threshold was ~10 pA. We routinely scrolled through detected events and visually rejected superimposed or spuriously detected events. Peak mPSC amplitudes were measured at the absolute maximum of the currents. Time to decay was calculated as the time from peak to 33% decay of the peak amplitude. Rise times were measured as the time elapsed from 10 to 90% of the peak mPSC amplitude. The charge transferred by each type of synaptic event (picocoulombs) was measured as the integrated area under averaged mPSCs. Curve fitting of mPSC decays (from peak to end) to single- or double-exponential equations was per-

formed on averaged traces with the simplex algorithm least squares exponential fitting method provided by MiniAnalysis software.

Postrecording identification of Renshaw cells. We identified Renshaw cells by the high density of cholinergic contacts immunoreactive for the vesicular acetylcholine transporter (VAChT) on their dendrites (Alvarez et al., 1999; Gonzalez-Forero and Alvarez, 2005). Recorded neurons were filled with neurobiotin (0.4% in pipette solution), and the slices were fixed in 4% paraformaldehyde for 30 min and then stored at 4°C in PBS. Immunohistochemistry was performed in the thick slices used for recording. To facilitate antibody penetration, the slices were dehydrated and rehydrated through graded alcohols and xylene, then washed in PBS, blocked with normal horse serum [1:10 in PBS and 0.3% Triton X-100 (TX)], and incubated free-floating for 24–48 hr at room temperature in primary antisera against VAChT (diluted 1:1000 in PBS and 0.3% TX). Thereafter, the slices were washed and incubated for 2 hr in streptavidin–Cy3 and FITC-coupled donkey anti-goat antibodies diluted in PBS and TX (1:50 dilutions; Jackson ImmunoResearch). Finally, the slices were mounted on glass slides and coverslipped with Vectashield (Vector Laboratories). Neurobiotin-labeled cells were first analyzed at low magnification to confirm their position in the Renshaw cell area (Gonzalez-Forero and Alvarez, 2005) and revealed the extension and orientations of dendritic trees and axonal arborizations. Then, the labeled neurons (Cy3) and VAChT immunofluorescence (FITC) were scanned at high magnification (60×2) with an Olympus Fluoview FX confocal microscope. Cell morphology and VAChT-IR bouton contacts were reconstructed from stacks of optical sections (1 μm step size). Recorded neurons were classified as Renshaw cells if they were contacted by a high number of VAChT-IR terminals on their somatodendritic surfaces. Only synaptic currents from identified Renshaw cells were analyzed.

Statistical analysis. ANOVA tests were run to compare the percentage of differences of electroneurographic activity between injected and noninjected nerves with time after the injection and to confirm the similitude of gephyrin clusters in the noninjected sides of different animals. Paired *t* tests were performed on animal means to compare average Renshaw cell gephyrin cluster areas in the noninjected and injected sides for each toxin and age. The average glycinergic and GABAergic peak amplitudes or decays were compared between control and experimental Renshaw cells with unpaired *t* tests (experimental and control Renshaw cell samples were obtained from slices obtained in several animals). Distribution histograms and cumulative curves of gephyrin cluster areas and inhibitory mPSCs recorded in experimental and control Renshaw cells were compared using Kolmogorov–Smirnov (K–S) tests. Data are expressed as mean ± SE. Significance for all statistical tests was set at $p < 0.05$. Statistics were run in SigmaStat version 2.0 or Statistica version 5.1.

Image composition and presentation. Figure composition and labeling were done in CorelDraw 8.0 or SigmaPlot 4.0. For presentation purposes, confocal images of gephyrin clusters were enhanced using a high Gauss filter (Image Pro-Plus). This filter improves visualization of fine detail in small fluorescent punctate structures. Measurements were done in the raw images with no postcapture modifications.

Results

Intramuscular TeNT and BoNT-A, respectively, increased and decreased motor axon output and muscle activity in neonatal rats

Neonatal rats show decreased sensitivity to clostridial toxins compared with adults (Pastor et al., 2003). To maximize toxin effects in neonates, we determined the largest dose for each toxin that injected intramuscularly in the gastrocnemius muscle of P5 rat pups was compatible with adequate survival (see Materials and Methods). Doses of 25 ng/kg TeNT and 30 ng/kg BoNT-A resulted in survival rates at P20 close to 90 and 80%, respectively. Toxin-treated neonates and nontreated littermates showed no significant differences in weight gain, suggesting normal overall development with these toxin doses. Animals that received injections at P5 with 25 ng/kg TeNT showed ipsilateral tetanic extension of the ankle within 24–48 hr after injection. Tetanic extension was clearly visible during the next 8–10 d and then slowly recovered. In contrast, animals that received injections of 30 ng/kg BoNT-A showed flaccid paralysis of the ankle joint that started within 24 hr after injection. BoNT-A effects began to recover ~6–8 d after injection (P11–P13). These short time courses of toxin-induced paralysis contrast with the long-lasting paralysis (15–20 d for TeNT and 1–3 months for BoNT-A) induced in adult animals (Sanna et al., 1993; Moreno-López et al., 1997; Gonzalez-Forero et al., 2003).

Next, we characterized toxin actions on NMJ neurotransmission and peripheral nerve motor axon activity. The degree and time course of NMJ block was estimated in rat pups of 7–21 d of age as the ratio of peak force amplitude evoked in the isolated gastrocnemius muscle after direct electrical stimulation of muscle fibers and after nerve stimulation (i.e., indirect stimulation) (Fig. 1*A–C*). Maximum force peak amplitudes after direct muscle stimulation were comparable in magnitude between injected and noninjected muscles. Nerve-induced muscle contractions in noninjected muscles or muscles injected with TeNT were 80–95% of the force generated by direct stimulation applied to the muscle (Fig. 1*A*,*B*), suggesting normal NMJ transmission. In contrast, muscle force produced by nerve simulation in BoNT-A-injected muscles was <5% of the force generated by direct muscle stimulation at P7 and recovered to ~50% by P21 (Fig. 1*B*,*C*). In conclusion, 30 ng/kg BoNT-A in neonatal rat pups induced NMJ blocks that partially recovered during the second postinjection week. TeNT exerted little or no action on NMJ transmission at this dose.

To characterize the time course of effects on ventral horn motor output, we compared motor axon activity recorded in peripheral nerves ipsilateral and contralateral to toxin injections. Branches of the tibial nerve innervating the gastrocnemius muscle in the injected and contralateral control sides were prepared for extracellular recordings of bilateral reflex nerve activity elicited by mechanical stimulation (firm rubbing with a glass rod) of the tail. The nerves were cut distal to recording sites to prevent contamination from muscle sensory afferent activity. Examples of raw extracellular recordings in control and treated nerves are shown in Figure 1, *D* and *E*. An average percentage of difference of the evoked activity in control and experimental sides was calculated for each animal from the areas under the curve of half-wave-rectified electroneurographic recordings. Three animals were analyzed with each toxin and at each postinjection date (6 hr and 1 d after a P5 toxin injection and then every 2 d until P19). TeNT-injected animals showed dramatic increases in motor response compared with the control side. In contrast, BoNT-A-treated nerves show depressed motor nerve responses (Fig. 1*D*,*E*). Significant changes in bilateral responses were detected from 1 to 10 d after injection (i.e., P15) after TeNT and from 6 hr to 12 d after injection (P17) in BoNT-A-treated animals (Fig. 1*F*) (two-way ANOVA; LSD test for *post hoc* comparisons; $p < 0.05$). Maximal response differences after TeNT peaked at 4–6 d after injection (P9–P11) and after BoNT-A peaked at 2–4 d after injection (P7–P9). Responses in toxin-injected and contralateral nerves were not significantly different 12 d after injection (P17–P19) for TeNT and 14 d (P19) for BoNT-A (Fig. 1*F*).

In summary, TeNT induced in neonates a chronic increase in motor output that was identified by tetanic extension of the ankle and by increases in motor nerve reflex response activity. In contrast, BoNT-A decreased motor output, best measured by dramatic reductions in reflex responses. In addition, BoNT-A effectively blocked NMJ neurotransmission. The peak effects of BoNT-A occurred faster than with TeNT, and the effects of both

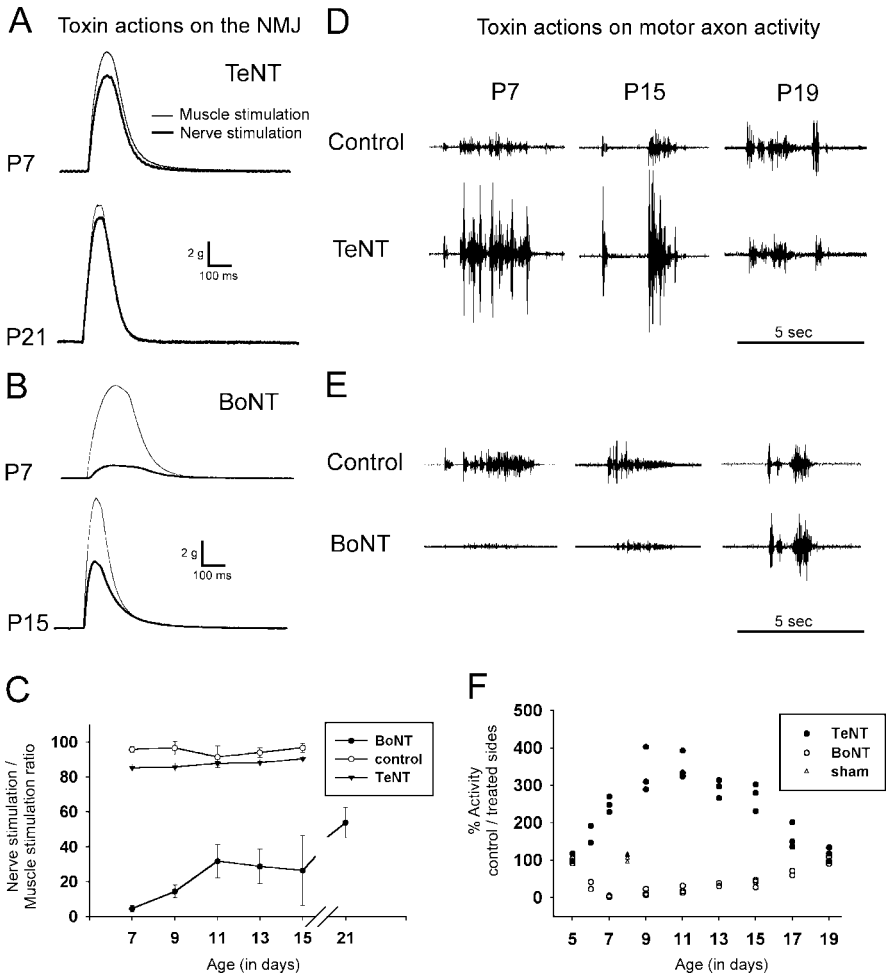

Figure 1. Peripheral actions of TeNT and BoNT-A. *A–C*, Toxin actions on the NMJ. *D–F*, Toxin actions on motoneuronal firing recorded by electroneurography of the tibial nerve. *A*, Representative tension recordings of gastrocnemius muscle contractions in P9 and P21 animals that received injections of 25 ng/kg TeNT after direct (applied to the muscle) and indirect (applied to the tibial nerve) stimulation. Muscle contractions are similar after either stimulation, suggesting unblocked neuromuscular transmission. *B*, Same as in *A*, but for P7 and P15 animals that received injections of 30 ng/kg BoNT-A. Profound neuromuscular transmission blockade occurred at P7 (muscle does not contract by stimulating the nerve) that partially recovered at P15. *C*, Time course of changes in indirect (nerve) to direct (muscle) stimulation tension-evoked ratios after treatment with clostridial neurotoxins. Control data are from the contralateral noninjected side. Two-way ANOVA indicates significant differences between BoNT-A treatment at all time points with respect to the control side (LSD for *post hoc* comparisons at a significance level of $p < 0.05$). *D*, *E*, Selected epochs of nerve discharge at P7, P15, and P19 in TeNT- and BoNT-A-treated animals in response to stimulation of the tail tip. Motor responses were increased in the TeNT-treated nerve and depressed after BoNT-A. *F*, Time course of changes in nerve activity responses expressed as a percentage of the control side for the same time interval. Tetanus or depressed firing developed over 2–4 d after treatment. Significant changes occur from P6 to P15 for TeNT and from P6 to P17 for BoNT-A treatment (two-way ANOVA; LSD test for *post hoc* comparisons; $p < 0.05$). Sham-operated animals measured at P8 show similar responses in both sides.

toxins recovered during the second week after injection, returning to control levels ~P19. It was thus expected that these changes in motor output recorded peripherally should reflect parallel central alterations in motor axon inputs onto Renshaw cells.

Gephyrin cluster size increase in Renshaw cells after TeNT and decrease after BoNT-A injections

Renshaw cells develop distinctively large gephyrin clusters on their cell bodies and proximal dendrites, and most cluster growth occurs between P10 and P20 (Geiman et al., 2000). We argued that any acceleration in gephyrin cluster growth could be best detected at P15, but if alterations were only expressed in more mature clusters, then they could be more noticeable at P20. Moreover, P15 is the oldest age at which inhibitory synaptic currents in Renshaw cells were reliably recorded in spinal cord slices (Gonzalez-Forero and Alvarez, 2005). We therefore analyzed gephyrin cluster sizes in Renshaw cells at P15 and P20 after unilateral injections of TeNT or BoNT-A at P5.

Renshaw cells were sampled in the ventral 200 μm of the spinal cord and identified by their calbindin immunoreactivity in sections containing at least 10 motoneurons retrogradely labeled from toxin-injected muscles (Fig. 2*A–C*). Renshaw cells were sampled randomly in control and experimental sides at low magnification, and then gephyrin clusters were imaged at high magnification with confocal microscopy. Renshaw cell somata and proximal dendrites exhibited a variety of gephyrin clusters from very small round puncta to large and bright clusters showing perforations or scalloped contours. Renshaw cells ipsilateral to TeNT-injected motor pools frequently displayed increased numbers of very large and bright clusters compared with Renshaw cells located in the contralateral side (Fig. 2*D*,*E*). In contrast, Renshaw cells ipsilateral to BoNT-A injections exhibited fewer large clusters (Fig. 2*F*).

Calbindin immunofluorescence was similar in the injected and noninjected sides of P15 and P20 TeNT-treated animals; however, it was reduced in the injected side of most BoNT-A-treated animals at P20 (four of six) and at P15 (three of four) (supplemental Fig. 2, available at www.jneurosci.org as supplemental material) (Sanna et al., 1993). The number of calbindin-IR neurons in the ventral 200 μm of laminas VII and IX (Renshaw cells) was, however, similar in both spinal cord sides in all of these animals. BoNT-A-injected animals analyzed at P15 contained some ventral neurons in the Renshaw cell area with weak calbindin immunofluorescence that was displaced to the periphery of cell somata (data not shown). Neurons with this calbindin immunofluorescence pattern were frequently covered by gephyrin clusters too dim to image. These clusters were unmeasurable with our techniques, and therefore these cells could not be analyzed. No such cells were encountered in TeNT-injected animals or in BoNT-treated animals analyzed at P20.

Quantitative analysis of gephyrin cluster areas showed an increase in gephyrin cluster size on Renshaw cells ipsilateral to TeNT injections and a decrease in BoNT-A-treated sides compared with their respective contralateral sides. We first calculated the average gephyrin cluster sizes of Renshaw cells sampled from toxin-injected and contralateral sides and performed paired comparisons within animals between toxin-injected and noninjected sides. An average percentage of change was then calculated

for each toxin and survival date (Fig. 3). In a second analysis, we pooled together all gephyrin clusters sampled for each toxin and age and constructed histogram distributions and cumulative probability functions of their areas (Fig. 4).

Renshaw cell gephyrin cluster area increased, on average, 18.4% in P15 TeNT-injected animals, from 0.24 ± 0.003 μm^2 contralateral to the TeNT-injected side (control) to 0.29 ± 0.021 μm^2 in ipsilateral experimental Renshaw cells ($n = 5$ animals; $n = 42$ control and 42 experimental Renshaw cells). At P20, the average increase in size was 28.4%. The average gephyrin cluster areas were 0.32 ± 0.020 μm^2 contralateral and 0.41 ± 0.019 μm^2 ipsilateral to the TeNT injections in P20 animals ($n = 4$ animals; $n = 54$ and 55 control and experimental Renshaw cells, respectively). Larger area estimates at P20 reflect the maturation of gephyrin cluster sizes on Renshaw cells with age (Geiman et al., 2000). Paired comparisons of gephyrin cluster areas indicated that differences in cluster size estimated in control Renshaw cells (contralateral) and in Renshaw cells ipsilateral to TeNT injections were significant at both ages (paired t test; $p < 0.05$) (Fig. 3*A*,*C*,*E*).

Average gephyrin cluster size decreased after BoNT-A injections. At P15, we calculated an average 17.7% decrease in gephyrin cluster size. Average gephyrin cluster areas decreased from 0.31 ± 0.009 μm^2 control to 0.25 ± 0.020 μm^2 ipsilateral to BoNT-A injections ($n = 4$ animals; $n = 45$ and 51 control and experimental Renshaw cells, respectively). Similar to TeNT experiments, differences after BoNT-A were larger at P20. In these animals, gephyrin cluster areas were decreased by 19.9%, on average, from 0.34 ± 0.010 μm^2 contralateral to 0.28 ± 0.022 μm^2 ipsilateral to BoNT-A injections ($n = 6$ animals; $n = 50$ and 53 control and experimental Renshaw cells, respectively). Differences in gephyrin cluster area after BoNT-A were also statistically significant at both ages (paired t test; $p < 0.05$) (Fig. 3*B*,*C*,*E*).

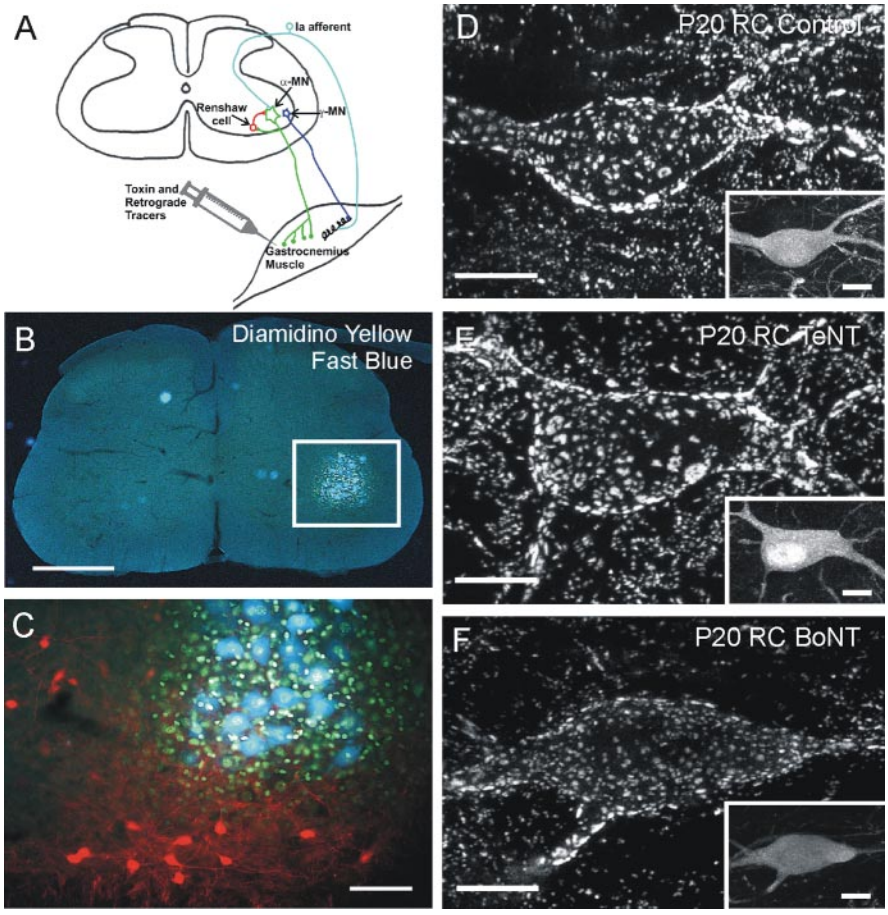

Figure 2. Experimental design and alterations of gephyrin cluster structure on Renshaw cells after TeNT or BoNT-A injections. *A*, Diagram illustrating the basic circuit between muscle and the spinal cord motor network targeted by peripherally administered clostridial toxins. Toxins and retrograde tracers were injected in the gastrocnemius muscle. BoNT-A affects NMJs at extrafusal and intrafusal muscle fibers, and some enters the retrograde transport toward the spinal cord. TeNT bypasses the NMJ and is retrogradely transported to the cell bodies, where it exerts it effects over inhibitory synapses on the motoneuron (MN) cell somas (see Discussion for details and references). *B*, Retrograde tracers (Fast Blue and Diamidino Yellow) were injected with each toxin or vehicle to identify spinal cord sections containing large numbers of affected motoneurons. The gastrocnemius motor pool is retrogradely labeled by Fast Blue (motoneuron somata) and Diamidino Yellow (motoneuron large nuclei). *C*, The region within the white box in *D* is magnified in *C*, and calbindin immunoreactivity is added to show Renshaw cells in the vicinity of toxin-treated motoneurons. Renshaw cells in sections containing >10 labeled motoneurons were sampled randomly for analysis from both injected (containing the labeled motoneurons) and contralateral sides (unlabeled, control). *D*, Confocal reconstruction of the surface of a Renshaw cell (RC) from the control side of a P20 animal. The proximal somatodendritic surface is covered with gephyrin clusters of different sizes and shapes, usually larger than clusters on processes of other neurons in the adjacent neuropil. *E*, *F*, Similar surface reconstructions of Renshaw cells (RC) from ventral horns containing TeNT-treated (*E*) or BoNT-A-treated (*F*) motoneurons. Calbindin immunoreactivity of these Renshaw cells is illustrated in their respective insets (bottom right). Several optical sections were superimposed to render *en face* views of gephyrin clusters covering the top surfaces of the neurons. All Renshaw cells exhibited large gephyrin clusters that easily distinguished them from other neurons; however, large clusters were more frequent in TeNT-treated Renshaw cells and less after BoNT-A. Scale bars: *B*, 500 μm; *C*, 100 μm; *D–F*, 10 μm; insets, 5 μm.

The individual areas of Renshaw cell gephyrin clusters always varied between two orders of magnitude (from 0.07 to >1.5 μm^2). Although large clusters are quite distinct and define Renshaw cells, smaller clusters (i.e., clusters <0.4 μm^2) always predominate (Geiman et al., 2000). Interestingly, gephyrin cluster size distribution histograms indicated that the proportion of small clusters (i.e., < 0.4 μm^2) decreased ipsilateral to the injection in TeNT-treated animals in favor of increasing the distribution skew toward larger gephyrin cluster sizes (Fig. 4*A*,*B*). Thus, cumulative probability functions of gephyrin cluster sizes were shifted toward larger values in the TeNT-treated side compared with the contralateral side. This shift was larger at P20 than at P15. The distribution histograms of gephyrin cluster sizes in Renshaw cells located in the ventral horns ipsilateral to BoNT-A injections showed opposite changes, the distribution histograms showed smaller percentages of gephyrin clusters of large size, and cumulative probability functions were shifted to the left, toward smaller size clusters. Changes in histogram distributions and curve shifts after BoNT-A were also more evident at P20. Changes in gephyrin cluster size distributions were significant in all cases ($p < 0.05$; K–S test). We concluded that TeNT increased the average gephyrin cluster size by specifically increasing the proportion of large size gephyrin clusters (>0.4 μm^2), whereas BoNT-A resulted in opposite changes.

Each gephyrin cluster represents the PSD of an independent synaptic complex, and frequently, several synaptic complexes are

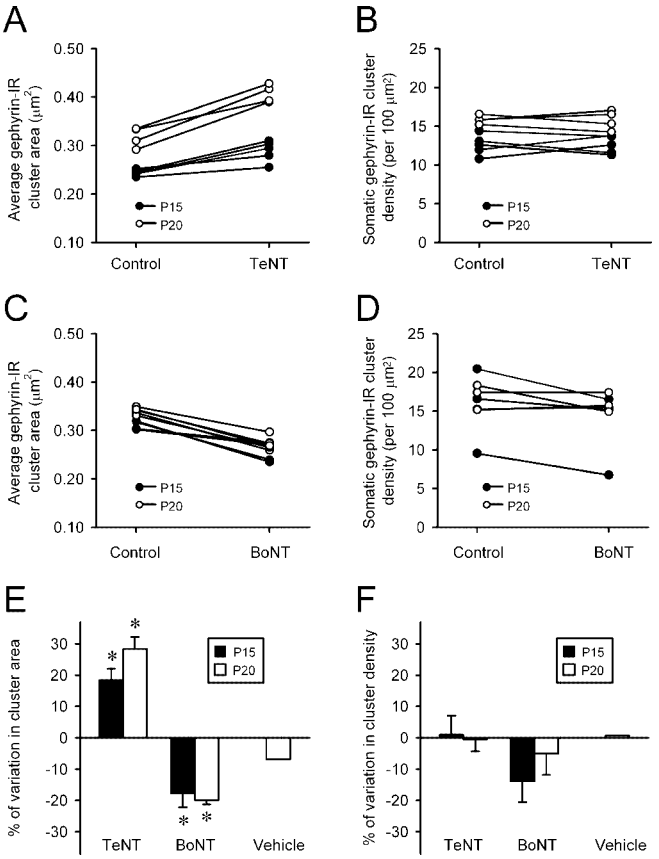

Figure 3. Effects of TeNT and BoNT-A on the development of gephyrin-IR clusters on Renshaw cells. *A*, *B*, Plots illustrating average cluster sizes (*A*) and densities (*B*) obtained from five P15 (●) and four P20 (○) TeNT-treated animals. Points connected by lines represent the average cluster areas or densities in the control (contralateral) and experimental (ipsilateral) side of the same animal. Cluster sizes and densities increased from P15 to P20. Gephyrin clusters on TeNT-treated Renshaw cells were always larger than on the control side, whereas no change was observed in cluster density. *C*, *D*, Same as in *A* and *B*, but for data obtained from four P15 and six P20 (only 3 in *D*) BoNT-A-treated animals. BoNT-A treatment had opposite effects on the cluster size development. The average cluster area in all of the animals was smaller on the BoNT-A-injected side, whereas cluster density remained unchanged relative to control, except for one P15 animal that was clearly different from the rest. *E*, *F*, Analysis of average changes (expressed as a percentage of variation; mean ± SE) in gephyrin cluster area (*E*) or density (*F*) on Renshaw cells induced by TeNT and BoNT-A treatments at P15 (■) and P20 (□). Gephyrin cluster areas significantly increased or declined on the treated side after TeNT or BoNT-A, respectively; cluster density was slightly reduced only in BoNT-A-injected animals. However, this difference was below the statistical significance level ($p > 0.05$). Asterisks indicate significant differences relative to the contralateral (untreated) side ($p < 0.05$; paired Student's *t* test).

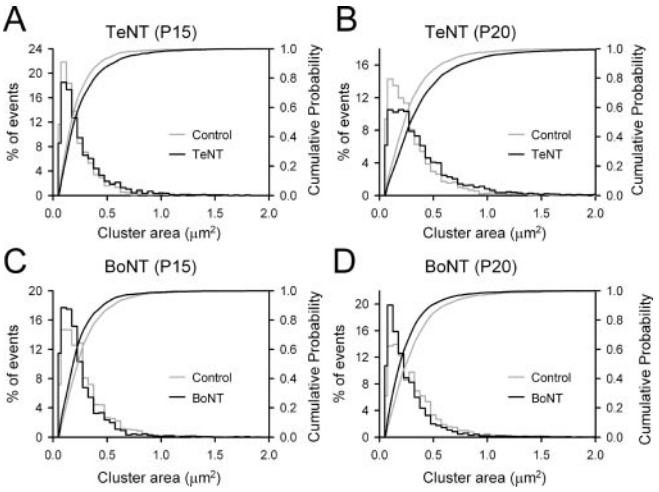

Figure 4. Gephyrin cluster size distributions are changed in opposite directions by TeNT and BoNT-A. *A*, *B*, Distribution histograms and cumulative probability functions of gephyrin cluster areas measured on Renshaw cells from five P15 (*A*) and four P20 (*B*) TeNT-treated animals. Data were obtained from 42 control (gray lines; $n = 2375$ clusters) and 42 experimental (black lines; $n = 2287$ clusters) Renshaw cells (RCs) at P15 (*A*) and from 55 control (gray lines; $n = 4870$ clusters) and 54 experimental (black lines; $n = 5167$ clusters) RCs at P20. *B*, *C*, Same as in *A* and *B*, but for RCs from BoNT-A-treated animals ($n = 4$ at P15 and $n = 6$ at P20). Data are pooled from 45 control (gray lines; $n = 2935$ clusters) and 51 experimental (black lines; $n = 2923$ clusters) RCs at P15 (*C*) and from 55 control (gray lines; $n = 4870$ clusters) and 53 experimental (black lines; $n = 5167$ clusters) RCs at P20 (*D*). Cumulative probability functions were progressively shifted to the right, and the area distributions were skewed toward larger sizes at the ages P15 and P20 after TeNT. In contrast, BoNT-A treatment caused opposite shifts to the right (lower cluster areas) in gephyrin cluster area distributions. All four distributions of gephyrin cluster sizes ipsilateral to the injected side were significantly different from contralateral control distributions ($p < 0.05$; K–S test). Bin width, 0.05 μm.

formed by individual boutons (Triller et al., 1985; Alvarez et al., 1997). Thus, increasing the number of synaptic complexes per bouton could compensate for a decrease in their individual sizes. However, the surface densities of gephyrin clusters (i.e., number of clusters per 100 μm^2 of somatic surface membrane) did not change after TeNT treatments at any survival date (paired *t* tests; $p > 0.05$) (Fig. 3*F*). There was a trend toward decreased densities in Renshaw cells ipsilateral to BoNT-A injections at P15, but it did not reach statistical significance ($p = 0.057$; paired *t* test). This trend was not observed at P20 ($p = 0.26$; paired *t* tests).

TeNT induced a significant increase in inhibitory currents in Renshaw cells

The morphological analyses described above suggest relatively small but significant changes in gephyrin clustering after altering motor nerve activity with clostridial toxins. Thus, we investigated the functional consequences of these structural changes by recording inhibitory (glycinergic and GABAergic) miniature synaptic currents (mPSCs) in Renshaw cells after altering motor axon activity. Motoneuron viability limits Renshaw cell recordings in spinal cord slices to the first two postnatal weeks (Gonzalez-Forero and Alvarez, 2005). Recorded neurons were neurobiotin filled and identified as Renshaw cells using histological criteria (Fig. 5) (Gonzalez-Forero and Alvarez, 2005). Neurons displaying many VAChT-IR contacts on their soma and dendrites were classified as Renshaw cells. VAChT-IR contacts occurred at higher density on dendritic segments at some distance from the cell body as shown for adult Renshaw cells (Fig. 5*B*,*D*) (Alvarez et al., 1999). All of the cells identified as Renshaw cells were located in the ventralmost 200 μm of laminas VII and IX (Geiman et al., 2000; Gonzalez-Forero and Alvarez, 2005). All of the cells had local dendritic arbors that extended little beyond 200 μm of the cell bodies, and in some cases, we revealed a local axon that targeted motoneuron pools (the cell shown in Fig. 5*A* is a good example). Some non-Renshaw cell interneurons and motoneurons were also recorded (Fig. 5*C*), but they were not analyzed further.

As reported previously, pharmacologically isolated spontaneous GABAergic/glycinergic mPSCs in Renshaw cells of this age have characteristics different from other neurons (Gonzalez-Forero and Alvarez, 2005). Renshaw cell GABAergic/glycinergic mPSCs are characterized by fast events (glycinergic) with larger than usual peak amplitudes, the presence of many slow events (GABAergic), and a relative high frequency of biphasic events with fast and slow components in their decays. In Renshaw cells sampled from the TeNT-treated side, the most obvious change

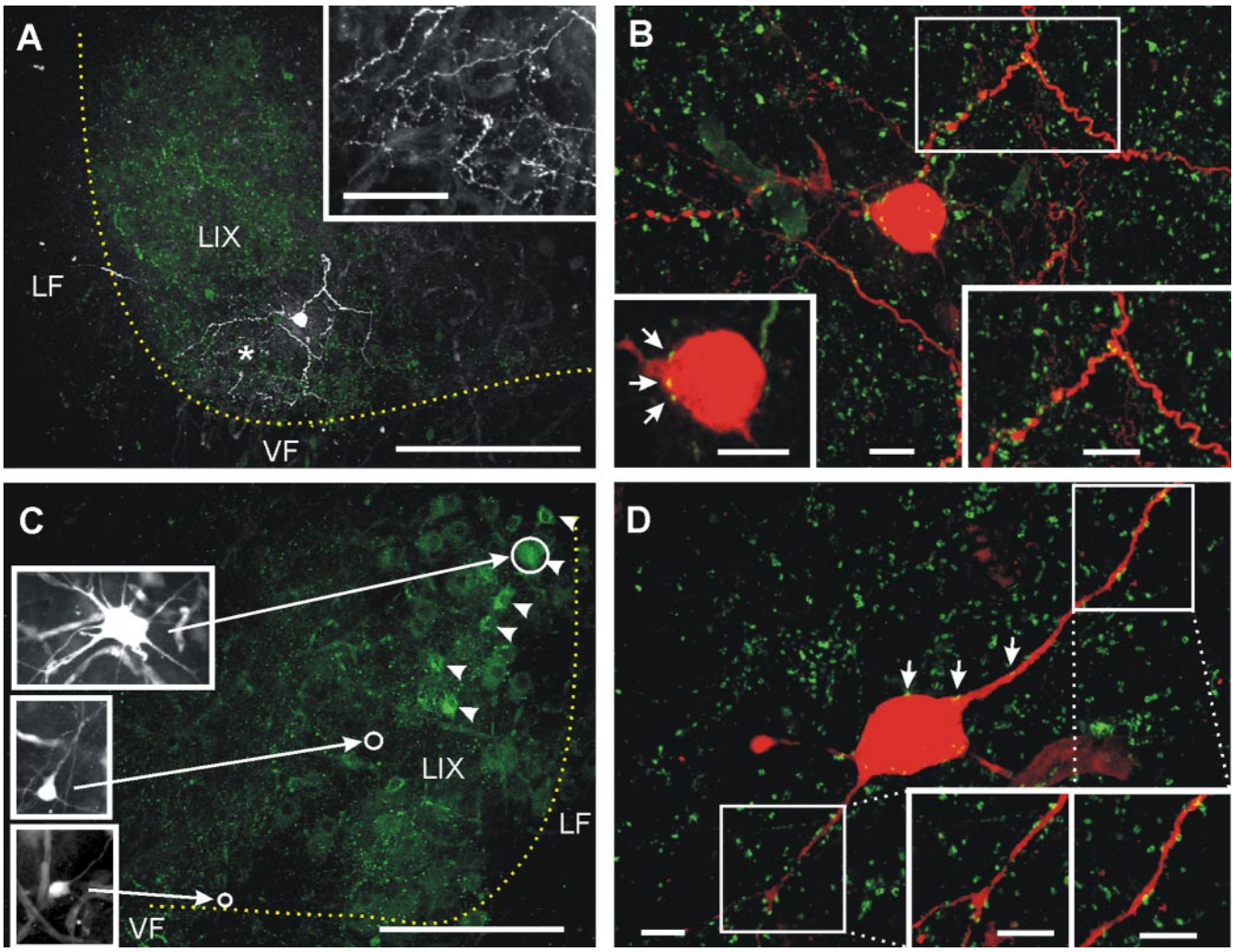

Figure 5. Anatomical characterization of recorded Renshaw cells. *A*, Selected low-magnification confocal optical planes through a 300-μm-thick slice of a P10 spinal cord containing a neurobiotin-labeled Renshaw cell (streptavidin–Cy3 is shown in white to better display details of its dendrites and axon) and VAChT-IR boutons (green; FITC). This image is from the control side of a TeNT-injected animal. VAChT immunoreactivity is weak inside motoneuron cell somas and very strong in C terminals in lamina IX (LIX) and surrounding Renshaw cells (Alvarez et al., 1999). This Renshaw cell had a profuse local axonal arborization that targeted ventral motor pools. Inset, Varicose axon collaterals from the region labeled with an asterisk in *A*. The yellow dotted line indicates the gray/white matter border. *B*, High-magnification image showing a partial reconstruction of the cell soma and dendrites of the Renshaw cell shown in *A* (white dot). VAChT-IR terminals appear in green. Many VAChT-IR boutons contact the cell soma (bottom left inset; arrows) and dendrites. The boxed dendritic region (bottom right) is shown at higher magnification in the bottom left inset. *C*, Low magnification of selected optical planes from the TeNT-injected side of a 300-μm-thick P9 spinal cord slice. VAChT-IR boutons appear as small dots in green (FITC). In addition, motoneuron somata containing retrogradely transported FITC–CTb are indicated with arrowheads. In this section, three neurons were recorded and labeled (open circles indicated the locations of the cell bodies). Cell body images of recorded cells are shown in the insets at the left. The neuron at the top is a motoneuron that also contained FITC–CTb. The neuron at the bottom corresponds to a Renshaw cell shown at higher magnification in *D*. The cell in the middle did not display VAChT-IR contacts or Renshaw cell characteristics and probably represents another kind of ventral interneuron. The yellow dotted line indicates the gray/white matter border as before. *D*, High magnification of the Renshaw cell in the TeNT-treated side of the slice shown in *C*. VAChT-IR contacts are indicated in the cell soma and proximal dendrites (arrows). The density of VAChT-IR contacts increases at some distance from the cell body (boxed dendritic regions shown in the indicated insets). The distribution of VAChT-IR contacts resembles that of adult Renshaw cells (Alvarez et al., 1999). LF, Lateral funiculs; VF, ventral funiculus; LIX, lamina IX. Scale bars: *A*, *C*, 200 μm; *B*, *D*, insets, 5 μm.

was an increase in the peak amplitude of the fast events and the fast component of mixed events (Fig. 6*A*). To quantitatively analyze mPSC alterations in Renshaw cells sampled contralateral ($n = 8$) and ipsilateral ($n = 8$) to the TeNT injection side, we obtained average traces of all mPSCs in each cell. These average currents included events with fast, slow, and mixed decays; thus, their decays were best fitted by the sum of two exponential functions (Fig. 6*B*). We measured the average current peak amplitude, the estimated fast and slow decay time constants (τ_f and τ_s, respectively), the ratio of the fast and slow components to the absolute current peak (A_f/A_s ratio), and the total charge under the average current curve (Fig. 6*C–F*). Significant increases in peak amplitude, A_f/A_s ratio, and total charge were detected in Renshaw cells ipsilateral to TeNT injections compared with contralateral control Renshaw cells ($p < 0.05$; Student's *t* test). Peak amplitudes increased by 78.9% from an average of 117.56 ± 10.87 pA in control compared with 210.31 ± 16.83 pA in the TeNT-treated side. Control Renshaw cell average peak amplitudes were similar to those reported previously in a different sample of noninjected animals at the same age (Gonzalez-Forero and Alvarez, 2005). In addition, A_f/A_s ratios almost doubled from a 3.36 ratio in control Renshaw cells to a 6.45 ratio in the TeNT-injected side (91.8% increase). This suggests that the fast component of the currents increased in size relative to the slower component. No significant differences were detected in the decay time constants of the fast ($\tau_f = 3.27 \pm 0.16$ msec in control and 3.57 ± 0.26 msec in the TeNT-injected side; $p = 0.35$; Student's *t* test) or slow ($\tau_s =$ 39.00 ± 2.31 msec in control and 48.21 ± 14.48 msec in the

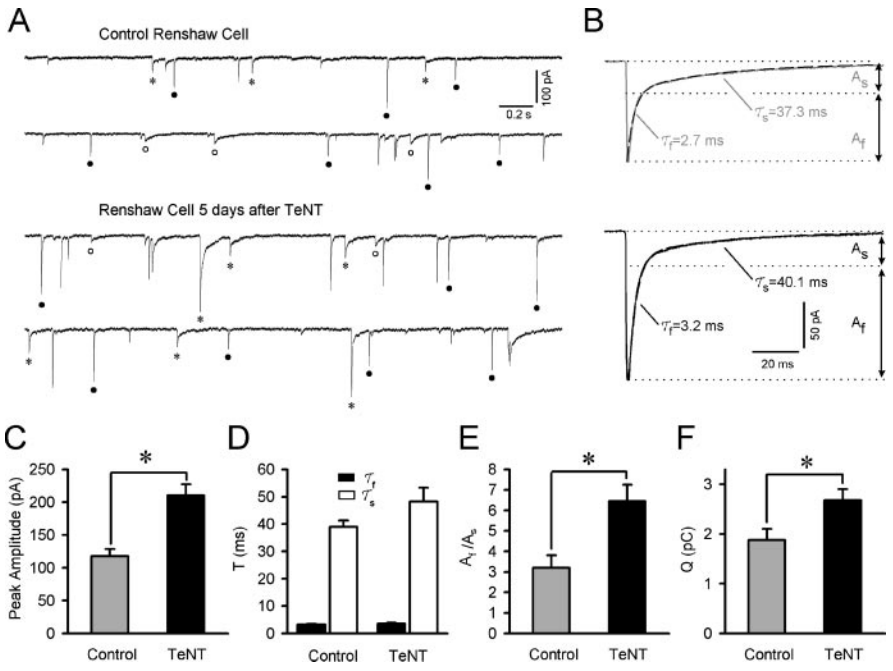

Figure 6. Inhibitory synaptic currents are upregulated in Renshaw cells located ipsilateral to TeNT injections. *A*, Traces of spontaneously occurring miniature "inhibitory" PSCs recorded from a P11 Renshaw cell in the control side (top traces) and from a P10 Renshaw cell recorded in the TeNT-injected side 5 d after injection (bottom traces). Neurons were voltage clamped at −75 mV, and mPSCs were isolated with TTX (1 μM), CNQX (10 μM), and D-tubocurarine (30 μM). Three different types of mPSCs could be identified: fast decaying (●), slow decaying (○), and mixed events (asterisks). Peak amplitudes of fast and mixed mPSCs were larger in TeNT-treated Renshaw cells. *B*, Average mPSCs of all of the types of events (fast decaying, slow decaying, and mixed events) from the cells illustrated in *A* during 5 min of continuous recordings. Decay phases of average mPSCs were always best fitted by double-exponential functions (superimposed dashed lines), in which τ_f and τ_s are the decay time constants of the "fast" and "slow" components, and A_f and A_s represent the relative contribution of the fast and slow components to the absolute peak amplitude. The averages of current traces in Renshaw cells in the TeNT-treated side (bottom trace) showed a large increase in the peak amplitude of the fast component and a slight slowing of the decay of the slow component. *C–F*, Histograms showing quantitative comparisons of peak amplitude (*C*), slow (τ_s) and fast (τ_f) decay time constants (*D*), A_f/A_s ratio (*E*), and charge transferred (*F*) for averaged mPSCs obtained in control ($n = 8$) and Renshaw cells in the TeNT-treated side ($n = 8$). The asterisks indicate significant differences between both groups ($p < 0.05$; Student's *t* test). The growth in amplitude of the fast component and the small lengthening of the slow component both significantly contributed to an increase in the charge transferred by the averaged mPSCs in Renshaw cells recorded in the TeNT-treated side.

TeNT-injected side; $p = 0.12$; Student's *t* test) components, although decays appeared somewhat longer ipsilateral to the TeNT injections. The amount of charge under the curve of average mPSCs increased by 42.4%, from 1.88 ± 0.63 pC in control to 2.68 ± 0.65 pC in the TeNT-injected side. These results strongly suggest that the underlying currents responsible for fast components (glycinergic) increased in size much more rapidly than those responsible for the slow components (GABAergic). To analyze each component separately, we isolated glycinergic mPSCs with bicuculline (10 μM) and GABAergic mPSCs with strychnine (0.25 μM).

As expected bicuculline-isolated glycinergic mPSCs showed a large increase in peak amplitude with no change in decay, rise times, or frequency (Fig. 7*A–D*). We quantitatively examined pharmacologically isolated glycinergic currents in 8 and 15 Renshaw cells contralateral and ipsilateral to TeNT injections. The distribution histograms of mPSC peak amplitudes (Fig. 7*E*) changed in similar ways to gephyrin clusters sizes after TeNT, and the proportion of small events was diminished in favor of a strong skew toward larger current amplitudes. As a result, the cellular average peak amplitude was significantly increased by 60.87% (127.14 ± 10.66 pA in control compared with 204.53 ± 42.81 pA in the TeNT-treated side; $p < 0.001$; Student's *t* test). The total charge was significantly increased in parallel (56.0% increase; 0.58 pC ± 0.05 pC in control to 0.90 ± 0.06 pC in the TeNT-injected side; $p = 0.003$; Student's *t* test). No significant differences were noted in decay ($\tau = 3.93 \pm 0.39$ msec in control and 4.3 ± 0.39 msec in the TeNT-injected side) or frequency (1.21 ± 0.29 Hz in control; 1.15 ± 0.25 msec in the TeNT-injected side).

Changes in GABAergic mPSCs after TeNT were more subtle. Qualitatively, GABAergic mPSCs frequently appeared augmented in peak amplitude (Fig. 8*A*) and with somewhat slower decays (Fig. 8*B*,*D*) ($\tau = 37.88 \pm 3.39$ msec in control and 46.86 ± 3.61 msec in the TeNT-injected side; $p = 0.13$; Student's *t* test) but similar rise times (Fig. 8*C*). Peak amplitude histograms and cumulative probability plots demonstrated statistically significant shifts in their distribution toward larger values ($p < 0.05$; K–S test); however, in our sample ($n = 5$ in both control and TeNT-treated sides), average cellular differences in peak amplitude did not reach statistical significance (44.05 ± 4.71 pA in control compared with 64.22 ± 11.15 pA in the TeNT-injected side; $p = 0.13$; Student's *t* test), most likely because of large cell-to-cell variability, particularly in the TeNT-treated side. Nevertheless, charge transfer was significantly increased by 49.86% in the TeNT-treated side (1.75 ± 0.16 pC in control to 2.63 ± 0.32 pC in the TeNT-injected side; $p = 0.04$), suggesting a change in GABAergic mPSC after TeNT treatment. It is interesting that the much longer time course of GABAergic events resulted in charge transfer alterations in GABAergic mPSCs after TeNT similar to those estimated for glycinergic mPSCs, despite much smaller changes in peak amplitude.

Discussion

The main findings of this study are that postsynaptic gephyrin cluster sizes and inhibitory mPSC peak amplitudes, particularly the glycinergic components, were modified in parallel in Renshaw cells after alteration of motoneuron activity. Inhibitory synapses on Renshaw cells display abundant GABA/glycine cotransmission (Geiman et al., 2002a; Gonzalez-Forero and Alvarez, 2005). Interestingly, synaptic GABAergic currents were affected to smaller degrees. Given the tight relationship between gephyrin, glycine receptor clustering (Kirsch et al., 1993; Feng et al., 1998; Kirsch and Betz, 1998; Kneussel et al., 1999, 2001; Meier et al., 2000), and postsynaptic glycinergic currents (Lim et al., 1999; Van Zundert et al., 2004), the most parsimonious explanation is that gephyrin/glycine receptor clustering on Renshaw cells is modulated by motor axon excitatory synaptic inputs and that this mechanism contributes to regulate postsynaptic current size. mPSC frequencies and gephyrin cluster surface densities did not significantly change, suggesting that the number of release sites (each opposed by a gephyrin cluster) and their release probabil-

ities were unaltered. However, the possibility that changes in neurotransmitter synaptic vesicle packing (Nabekura et al., 2004) also contributed to postsynaptic current alterations remained untested in these experiments.

Experimental model

Motor axon inputs on Renshaw cells were likely modified after TeNT and BoNT-A intramuscular injections altered motoneuron firing. The known mechanisms of action of these toxins explain well their effects in our neonatal rat model. TeNT injected intramuscularly in adults bypasses the NMJ and is retrogradely transported to motoneuron somata (Price et al., 1975), where it transynaptically translocates to presynaptic terminals (Schwab and Thoenen, 1976) and preferentially blocks neurotransmitter release from inhibitory synapses by cleaving synaptobrevin, a component of the soluble *N*-ethylmaleimide-sensitive factor attachment protein (SNAP) receptor (SNARE) complex (Schiavo et al., 1992). Thus, TeNT provokes central disinhibition, α-motoneuron tetanic firing, and spastic muscle contraction (Brooks et al., 1957). γ-Motoneurons are also released from inhibition, inducing a γ-bias that elevates Ia afferent firing and further increases α-motoneuron excitation (Takano and Kano, 1973). In contrast, BoNT-A evokes flaccid paralysis by blocking ACh release at the NMJ after cleaving SNAP25, another SNARE protein (Blasi et al., 1993; Schiavo et al., 1993). Motoneuron excitatory drive is further decreased after BoNT-A poisoning by muscle spindle unloading (Rosales et al., 1996). In addition, retrogradely transported BoNT-A (Wiegand and Wellhöner, 1974) can enter intraspinal motor axon recurrent collaterals and could block ACh release at motor axon–Renshaw cell synapses. Together, these actions should reduce motoneuron inputs on Renshaw cells after BoNT-A peripheral injections. Decreased Renshaw cell calbindin immunoreactivity after BoNT-A injections also suggested reduced excitatory activity in these cells (Sanna et al., 1993).

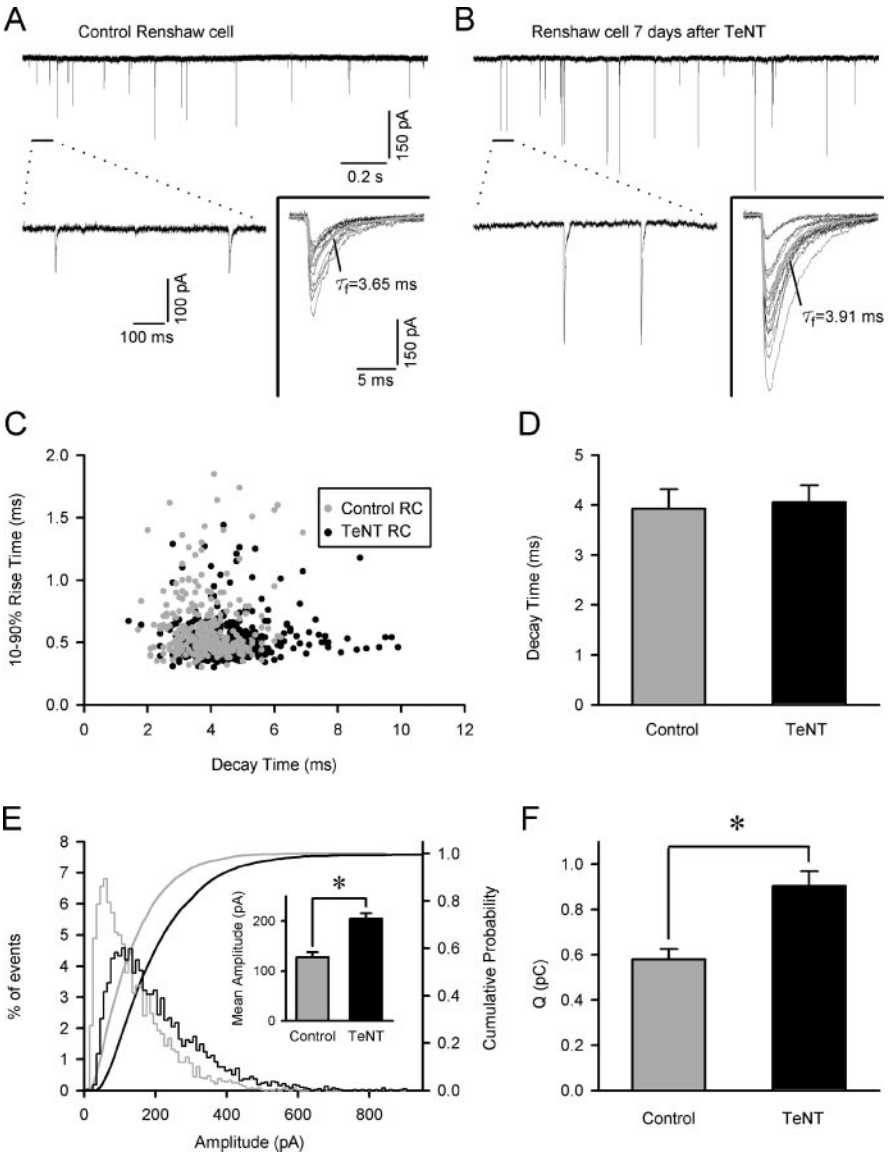

Figure 7. Peak amplitude of glycinergic mPSC increases in Renshaw cells after TeNT treatment. *A*, *B*, Glycinergic mPSCs recorded in the presence of TTX, CNQX, D-tubocurarine, and bicuculline (10 μM) from control P12 (*A*) and experimental P9 (*B*) Renshaw cells recorded 7 and 4 d after TeNT injection, respectively. The bottom traces display at a longer time scales the segments of recordings indicated in the top traces. The insets represent the superimposition of the individual events displayed in the top traces and their average (gray). Decays were well fitted by a single-exponential function to the average traces. The estimated decay time constants (τ) are also indicated. In Renshaw cells recorded in the TeNT-treated side, glycinergic mPSCs increase in peak amplitude without significant changes in the decay time course. *C*, Relationships between the 10–90% rise time to decay time of individual glycinergic mPSCs recorded from the control (gray dots) and TeNT-treated Renshaw cells (black dots) illustrated in *A* and *B*. No correlations were observed between both parameters ($r < 0.1$). *D*, Comparison of average (means ± SE) glycinergic mPSC decay times (to 33% of peak amplitude) from control ($n = 8$) and TeNT-treated Renshaw cells ($n = 15$). No significant differences ($p = 0.80$; Student's *t* test) were found. *E*, Histogram distribution and cumulative probability functions of glycinergic mPSC amplitudes for the same cells as in *D*. The amplitude histogram was skewed toward higher values, and the cumulative distributions significantly shifted to the right in the TeNT-treated side ($p < 0.05$; K–S test). Bin width, 10 pA. Inset, Mean peak amplitude values of glycinergic mPSCs were significantly different in Renshaw cells recorded from the TeNT-treated and control sides. *F*, Average charge transfer of glycinergic mPSCs in control and experimental Renshaw cells. Large amplitude glycinergic events contribute to a higher transfer of inhibitory charge into Renshaw cells located in the TeNT-treated side. The asterisks in *E* and *F* denote significant differences between TeNT-treated and control groups ($p < 0.05$; Student's *t* test).

Gephyrin cluster and glycinergic current alterations after changes in motor firing

By exploiting the favorable signal/noise ratio of gephyrin immunoreactivity to measure large numbers of immunofluorescent inhibitory PSDs (Triller et al., 1985; Alvarez et al., 1997), we were able to detect significant trends within their large structural variability. Nevertheless, cluster area measurements were limited by resolving power and tissue diffraction, being less accurate in smaller clusters. Thus, the smaller gephyrin clusters measured with immunofluorescence were larger than the smaller patches detected with electron microscopy (Alvarez et al., 1997). This could result in size overestimation of a proportion of small clusters. Because the number of small clusters decreased after TeNT and increased after BoNT-A, possible measuring errors in the population of small clusters could underestimate the increase in av-

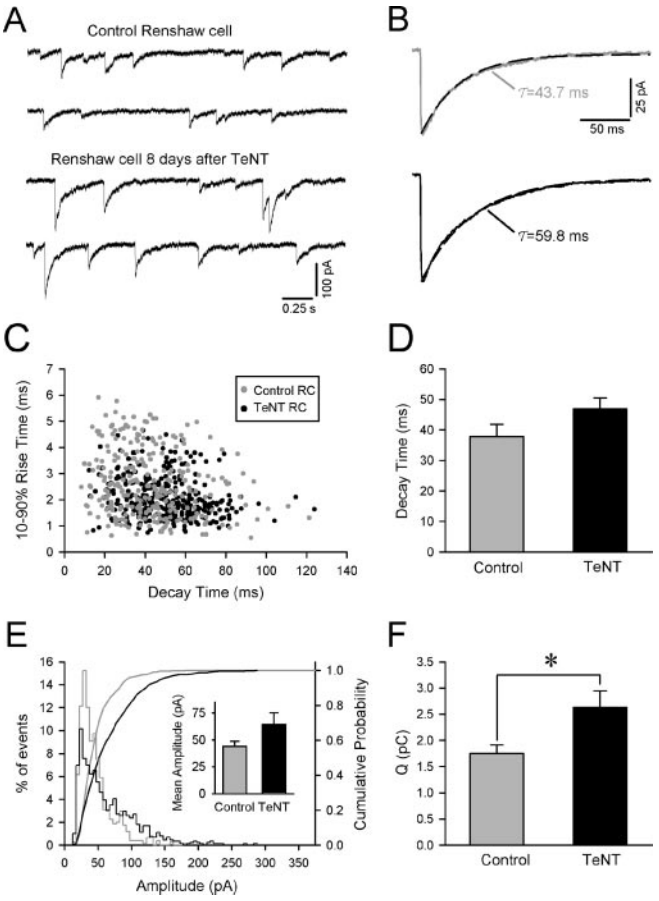

Figure 8. Variations in the kinetics and amplitude of GABAergic mPSCs after TeNT injections. *A*, Representative traces from a control P12 Renshaw cell and a TeNT-treated P13 Renshaw cell showing spontaneous isolated GABAergic mPSCs. Note a greater incidence of GABAergic mPSCs of larger amplitude and longer decays in the TeNT-treated side. *B*, Average current traces of GABAergic mPSCs obtained in the control and experimental Renshaw cells illustrated in *A*. The decay phase was best fitted with monoexponential functions. The decay time constant and peak amplitude values were somewhat higher in the TeNT-treated Renshaw cell. *C*, Ten to ninety percent rise time to decay time plots of GABAergic mPSCs obtained from the control (gray dots; $n = 327$ events) and TeNT-treated Renshaw cells (black dots; $n = 320$ events) shown in *A*. No correlations between both parameters were found ($r < 0.3$). Both distributions widely overlapped. *D*, Average GABAergic mPSC decay times (mean ± SE) in control ($n = 5$) and TeNT-treated Renshaw cells ($n = 5$). TeNT did not affect mean decays of GABAergic mPSCs ($p = 0.13$; Student's *t* test). *E*, Distribution histogram and cumulative probability functions of GABAergic mPSC peak amplitudes for five Renshaw cells recorded in the control side (gray lines; $n = 749$ events) and Renshaw cells recorded in the TeNT-treated side (black lines; $n = 1513$ events). Inset, Comparison of mean GABA mPSC peak amplitudes. Although TeNT significantly affected peak amplitude distributions ($p < 0.05$; K–S test), resulting in a prominent skew toward large amplitude events, statistical differences in their mean values were not reached ($p = 0.13$; Student's *t* test). *F*, Comparison of charge transfer (*Q*) by averaged GABAergic mPSCs in Renshaw cells recorded from the control and TeNT-treated sides. The combination of changes in amplitude and decay resulted in a significant increase in the charge transferred by GABAergic mPSCs in Renshaw cells located in the TeNT-treated side. The asterisk indicates significant differences ($p < 0.05$; Student's *t* test).

erage size after TeNT and the decrease after BoNT-A. However, they do not affect conclusions on the direction of change of gephyrin clustering.

Structural changes were paralleled by large alterations in synaptic currents. In agreement, previous comparisons of postsynaptic structure with functional synaptic parameters suggested that a 20% change in gephyrin cluster or inhibitory PSD area correlates with 1.5 to 3-fold differences in postsynaptic current amplitudes (Nusser et al., 1997, 1998; Lim et al., 1999). Similarly, during normal postnatal development, Renshaw cell gephyrin cluster areas increase by 86% from P5 to P15 (Geiman et al., 2000), whereas glycinergic mPSC peak amplitudes increase 230% in the same period (Gonzalez-Forero and Alvarez, 2005). One possible explanation for the relatively small structural changes that correlate with larger functional modifications is that inhibitory receptors could be packed at higher densities in larger PSDs. In fact, larger gephyrin clusters consistently display brighter immunofluorescence, and larger PSDs usually contain higher densities of receptors (Nusser et al., 1998; Takumi et al., 1999).

Our results suggest that motor synaptic inputs modulate gephyrin cluster maturation and inhibitory synaptic currents on Renshaw cells during postnatal development. Such a mechanism could produce the specific gephyrin clustering patterns found on adult Renshaw cells while adjusting inhibitory strength to the characteristics of convergent excitatory inputs. Generalization of this principle could also explain the somatodendritic gradients in gephyrin cluster size reported in other spinal neurons (Alvarez et al., 1997). Previous work in motoneurons suggested that Ia afferent EPSPs are larger in distal dendrites (Iansek and Redman, 1973; Jack et al., 1981), and distal PSDs opposite to Ia afferents were consistently larger (Pierce and Mendell, 1993). Similarly, recordings in CA1 dendrites suggested a scaling of excitatory synaptic currents with dendritic distance as a result of the accumulation of larger numbers of postsynaptic receptors at distal synapses (Magee and Cook, 2000; Andrasfalvy and Magee, 2001). Thus, larger gephyrin clusters in distal dendrites could be related to the presence of larger EPSPs.

Peak amplitude of GABAergic currents was less affected

$GABA_A$ receptor clustering has been related to gephyrin (Craig et al., 1996; Essrich et al., 1998; Sassoe-Pognetto and Fritschy, 2000), and activity has been shown to modify postsynaptic $GABA_A$ receptor numbers in forebrain synapses lacking postsynaptic glycine receptors (Nusser et al., 1998; Kilman et al., 2002; Marty et al., 2004). In our study, $GABA_A$ mPSC peak amplitudes were enhanced less than glycinergic mPSCs, perhaps suggesting a weaker relationship between gephyrin and the postsynaptic accumulation of $GABA_A$ receptors, compared with glycine receptors. Similar conclusions were reached comparing the developmental maturation of gephyrin clusters and postsynaptic currents on Renshaw cells (Gonzalez-Forero and Alvarez, 2005). Analyses in gephyrin knock-out mice also suggest that the relationship between gephyrin and $GABA_A$ receptor clustering is less tight than previously believed (Fischer et al., 2000; Kneussel et al., 2001; Levi et al., 2004) and that manipulation of gephyrin clustering through cytoskeletal disruption affects more profoundly glycinergic than $GABA_A$ postsynaptic currents (Van Zundert et al., 2004). Moreover, $GABA_A$ receptor clustering is gephyrin independent during early synaptogenesis (Dumoulin et al., 2000; Danglot et al., 2003; Levi et al., 2004), and a recent study indicated that postsynaptic $GABA_A$ receptor numbers and currents are better related to the abundance of specific gephyrin isoforms than to overall gephyrin clustering (Meier and Grantyn, 2004). Interestingly, GABAergic currents in Renshaw cells are mediated by the $\alpha3/\alpha5$ subunit containing $GABA_A$ receptors and result in long decays (Geiman et al., 2002a; Gonzalez-Forero and Alvarez, 2005), therefore comparatively smaller increases in GABAergic synaptic current peak amplitude resulted in total charge transfer increases similar to glycinergic currents. Therefore, it might not be necessary to recruit large numbers of $GABA_A$ receptors to significantly strengthen this component of the inhibitory current.

Modulation of inhibitory synapses by excitatory afferent activity

A number of recent results suggest that excitatory activity modulates the maturation of inhibitory synapses. Chronic NMDA exposure accelerated development of GABAergic inhibition in superior colliculus (Aamodt et al., 2000), and induction of epileptic activity in hippocampal neurons recruited more $GABA_A$ receptors and increased GABAergic miniature IPSCs (mIPSCs) (Otis et al., 1994; Nusser et al., 1998). Conversely, decreased activity in neocortical cultures reduced postsynaptic mIPSC amplitudes and $GABA_A$ receptor immunofluorescence (Kilman et al., 2002). Similarly, alterations of network activity in embryonic or neonatal spinal cords homeostatically regulated the strength of GABAergic synapses (Chub and O'Donovan, 1998; Rosato-Siri et al., 2002). At Renshaw cell mixed inhibitory synapses, the action of excitatory activity was more pronounced on the glycinergic component compared with GABAergic currents, and it was accompanied by increased gephyrin clustering.

The intracellular mechanisms that could mediate heterosynaptic modulation of inhibitory synaptic structure by excitatory synaptic activity are not clear. Gephyrin accumulates at membrane loci undergoing depolarization subsequent to the activation of unclustered inhibitory receptors by a mechanism dependent on Ca^{2+} entry through voltage-gated channels (Kirsch and Betz, 1998). Interestingly, gephyrin clustering continues at postnatal times in which inhibitory receptors no longer cause depolarization (Geiman et al., 2000). During this phase, Ca^{2+}-dependent gephyrin clustering could be triggered by local activity in excitatory synapses. Excitatory synapses can also interact with inhibitory synapse development through activation of metabotropic receptors (Meier et al., 2002) or release of trophic factors like brain-derived neurotrophic factor (Rutherford et al., 1997; Seil and Drake-Baumann, 2000; Aguado et al., 2003; Marty et al., 2004). These mechanisms, alone or in combination, could therefore adjust the balance between inhibition and excitation and contribute to homeostatic regulation of inhibitory synapses (for review, see Turrigiano and Nelson, 2004). Nevertheless, homeostatic mechanisms are usually interpreted as neuron-wide alterations, while gephyrin clusters remain very variable along the membranes of individual neurons. Therefore, models based on fine regulation of inhibitory synaptic strength within discrete compartments of the neuronal surface could better explain site-to-site variations of inhibitory synapse structure and strength.

References

Aamodt SM, Shi J, Colonesse MT, Veras W, Constantine-Paton M (2000) Chronic NMDA exposure accelerates development of GABAergic inhibition in the superior colliculus. J Neurophysiol 83:1580–1591.

Aguado F, Carmona MA, Pozas E, Aguilo A, Martinez-Guijarro FJ, Alcantara S, Borrell V, Yuste R, Ibanez CF, Soriano E (2003) BDNF regulates spontaneous correlated activity at early developmental stages by increasing synaptogenesis and expression of the K+/Cl− co-transporter KCC2. Development 130:1267–1280.

Alvarez FJ, Dewey DE, Harrington DA, Fyffe REW (1997) Cell-type specific organization of glycine receptor clusters in the mammalian spinal cord. J Comp Neurol 379:150–170.

Alvarez FJ, Dewey DE, McMillin P, Fyffe REW (1999) Distribution of cholinergic contacts on Renshaw cells in the rat spinal cord: a light microscopic study. J Physiol (Lond) 515:787–797.

Alvarez FJ, González-Forero D, Geiman E, Pastor AM (2004) Gephyrin clustering and postsynaptic glycinergic currents increase in Renshaw cells after enhancing motor axon inputs with tetanus neurotoxin. Soc Neurosci Abstr 30:838.8.

Andrasfalvy BK, Magee JC (2001) Distance-dependent increase in AMPA receptor number in the dendrites of adult hippocampal CA1 pyramidal neurons. J Neurosci 21:9151–9159.

Antal M, Freund TF, Polgar E (1990) Calcium-binding proteins, parvalbumin- and calbindin-D28k-immunoreactive neurons in the rat spinal cord and dorsal root ganglia: a light and electron microscopic study. J Comp Neurol 295:467–484.

Arvidsson U, Ulfhake B, Cullheim S, Ramírez V, Shupliakov O, Hökfelt T (1992) Distribution of calbindin D28k-like immunoreactivity (LI) in the monkey ventral horn: do Renshaw cells contain calbindin D28k-LI? J Neurosci 12:718–728.

Blasi J, Chapman ER, Link E, Binz T, Yamasaki S, deCamilli P, Sudhoff TC, Niemann H, Jahn R (1993) Botulinum neurotoxin A selectively cleaves the synaptic protein SNAP-25. Nature 365:160–163.

Brooks VB, Curtis DR, Eccles JC (1957) The cation of tetanus toxin on the inhibition of motoneurons. J Physiol (Lond) 135:655–672.

Carr PA, Alvarez FJ, Leman EA, Fyffe REW (1998) Calbindin D28k expression in immunohistochemically identified Renshaw cells. NeuroReport 9:2657–2661.

Chub N, O'Donovan MJ (1998) Blockade and recovery of spontaneous rhythmic activity after application of neurotransmitter antagonists to spinal networks of the chick embryo. J Neurosci 18:294–306.

Craig AM, Banker G, Chang W, McGarth ME, Serpinskaya AS (1996) Clustering of gephyrin at GABAergic but ot glutamatergic synapses in cultured rat hippocampal neurons. J Neurosci 16:3166–3177.

Danglot L, Triller A, Bessis A (2003) Association of gephyrin with synaptic and extrasynaptic GABAA receptors varies during development in cultured hippocampal neurons. Mol Cell Neurosci 23:264–278.

Dumoulin A, Levi S, Riveau B, Gasnier B, Triller A (2000) Formation of mixed glycine and GABAergic synapses in cultured spinal cord neurons. Eur J Neurosci 12:3883–3892.

Eccles JC, Fatt P, Koketsu K (1954) Cholinergic and inhibitory synapses in a pathway from motor-axon collaterals to motoneurones. J Physiol (Lond) 126:524–562.

Essrich C, Lorez M, Benson JA, Fritschy JM, Luscher B (1998) Postsynaptic clustering of major $GABA_A$ receptor subtypes requires the γ2 subunit and gephyrin. Nat Neurosci 1:563–571.

Fallah Z, Clowry GJ (1999) The effect of a peripheral nerve lesion on calbindin D28K immunoreactivity in the cervical ventral horn of developing and adult rats. Exp Neurol 156:111–120.

Feng G, Tintrup H, Kirsch J, Nichol MC, Kuhse J, Betz H, Sanes JR (1998) Dual requirement for gephyrin in glycine receptor clustering and molybdoenzyme activity. Science 282:1321–1324.

Fischer F, Kneussel M, Tintrup H, Haverkamp S, Rauen T, Betz H, Wassle H (2000) Reduced synaptic clustering of GABA and glycine receptors in the retina of the gephyrin null mutant mouse. J Comp Neurol 427:643–648.

Geiman EJ, Knox MC, Alvarez FJ (2000) Postnatal maturation of gephyrin/glycine receptor clusters on developing Renshaw cells. J Comp Neurol 426:130–142.

Geiman EJ, Zheng W, Fritschy JM, Alvarez FJ (2002a) Glycine and $GABA_A$ receptor subunits on Renshaw cells: relationship with presynaptic neurotransmitters and postsynaptic gephyrin clusters. J Comp Neurol 444:275–289.

Geiman EJ, Pastor AM, Alvarez FJ (2002b) Motoneuron excitatory input influences gephyrin cluster size and calbindin immunoreactivity on Renshaw cells. Soc Neurosci Abstr 28:245.6.

Gonzalez-Forero D, Alvarez FJ (2005) Differential postnatal maturation of $GABA_A$, glycine receptor and mixed synaptic currents in Renshaw cells and ventral spinal interneurons. J Neurosci, in press.

Gonzalez-Forero D, de la Cruz RR, Delgado-Garcia JM, Alvarez FJ, Pastor AM (2003) Functional alterations of cat abducens neurons after peripheral tetanus neurotoxin injection. J Neurophysiol 89:1878–1890.

Iansek R, Redman SJ (1973) The amplitude, time course and charge of unitary excitatory post-synaptic potentials evoked in spinal motoneurone dendrites. J Physiol (Lond) 234:665–688.

Jack JJ, Redman SJ, Wong K (1981) The components of synaptic potentials evoked in cat spinal motoneurones by impulses in single group Ia afferents. J Physiol (Lond) 321:65–96.

Kilman V, van Rossum MCW, Turrigiano GG (2002) Activity deprivation reduces miniature IPSC amplitude by decreasing the number of postsynaptic $GABA_A$ receptors clustered at neocortical synapses. J Neurosci 22:1328–1337.

Kirsch J, Betz H (1998) Glycine-receptor activation is required for receptor clustering in spinal neurons. Nature 392:717–720.

Kirsch J, Wolters I, Triller A, Betz H (1993) Gephyrin antisense oligonucle-

otides prevent glycine receptor clustering in spinal neurons. Nature 366:745–748.
Kneussel M, Brandstätter JH, Laube B, Stahl S, Muller U, Betz H (1999) Loss of postsynaptic $GABA_A$ receptor clustering in gephyrin-deficient mice. J Neurosci 19:9289–9297.
Kneussel M, Brandstätter JH, Gasnier B, Feng G, Sanes JR, Betz H (2001) Gephyrin-independent clustering of postsynaptic $GABA_A$ receptor subtypes. Mol Cell Neurosci 17:973–982.
Levi S, Logan SM, Tovar KR, Craig AM (2004) Gephyrin is critical for glycine receptor clustering but not for the formation of functional GABAergic synapses in hippocampal neurons. J Neurosci 24:207–217.
Lim R, Alvarez FJ, Walmsley B (1999) Quantal size is correlated with receptor cluster area at glycinergic synapses in the rat brainstem. J Physiol (Lond) 516:505–512.
Magee JC, Cook EP (2000) Somatic EPSP amplitude is independent of synapse location in hippocampal pyramidal neurons. Nat Neurosci 3:895–903.
Marty S, Wehrle R, Sotelo C (2004) Neuronal activity and brain-derived neurotrophic factor regulate the density of inhibitory synapses in organotypic slice cultures of postnatal hippocampus. J Neurosci 20:8087–8095.
McDonough SM, Clowry GJ, Miller S, Eyre JA (2001) Reciprocal and Renshaw (recurrent) inhibition are functional in man at birth. Brain Res 899:66–81.
Meier J, Grantyn R (2004) A gephyrin-related mechanism restraining glycine receptor anchoring at GABAergic synapses. J Neurosci 24:1398–1405.
Meier J, Meunier-Durmort C, Forest C, Triller A, Vannier C (2000) Formation of glycine receptor clusters and their accumulation at synapses. J Cell Sci 113:2783–2795.
Meier J, Jüttner R, Kirischuk S, Grantyn R (2002) Synaptic anchoring of glycine receptors in developing collicular neurons under control of metabotropic glutamate receptor activity. Mol Cell Neurosci 21:324–340.
Moreno-López B, de la Cruz RR, Pastor AM, Delgado-García JM (1997) Effects of botulinum neurotoxin type A on abducens motoneurons in the cat: alterations of discharge patterns. Neuroscience 81:437–455.
Nabekura J, Katsurabayashi S, Kakazu Y, Shibata S, Matsubara A, Jinno S, Mizoguchi Y, Sasaki A, Ishibashi H (2004) Developmental switch from GABA to glycine release in single central synaptic terminals. Nat Neurosci 7:17–23.
Nusser Z, Cull-Candy S, Farrant M (1997) Differences in synaptic $GABA_A$ receptor number underlie variation in GABA mini amplitude. Neuron 19:697–709.
Nusser Z, Hájos N, Somogyi P, Mody I (1998) Increased number of synaptic $GABA_A$ receptors underlies potentiation at hippocampal inhibitory synapses. Nature 395:172–177.
Oleskevich S, Alvarez FJ, Walmsley B (1999) Glycinergic miniature synaptic currents and receptor cluster sizes differ between spinal cord interneurons. J Neurophysiol 82:312–319.
Otis TS, De Koninck Y, Mody I (1994) Lasting potentiation of inhibition is associated with an increased number of gamma-aminobutyric acid type A receptors activated during miniature inhibitory postsynaptic currents. Proc Natl Acad Sci USA 91:7698–7702.
Pastor AM, Mentis GZ, de la Cruz RR, Diaz E, Navarrete R (2003) Increased electrotonic coupling in spinal motoneurons after transient botulinum neurotoxin paralysis in the neonatal rat. J Neurophysiol 89:793–805.
Pierce JP, Mendell LM (1993) Quantitative ultrastructure of Ia boutons in the ventral horn: scaling and positional relationships. J Neurosci 13:4748–4763.
Price DL, Griffin J, Young A, Peck K, Stocks A (1975) Tetanus toxin: direct evidence for retrograde intraaxonal transport. Science 188:945–947.
Renshaw B (1946) Central effects of centripetal impulses in axons of spinal ventral roots. J Neurophysiol 9:191–204.
Rosales RL, Arimura K, Takenaga S, Osame M (1996) Extrafusal and intrafusal muscle effects in experimental botulinum toxin-A injection. Muscle Nerve 19:488–496.
Rosato-Siri M, Grandolfo M, Ballerini L (2002) Activity-dependent modulation of GABAergic synapses in developing rat spinal networks in vitro. Eur J Neurosci 16:2123–2135.
Rutherford LC, DeWan A, Lauer HM, Turrigiano GG (1997) Brain-derived neurotrophic factor mediates the activity-dependent regulation of inhibition in neocortical cultures. J Neurosci 17:4527–4535.
Sanna PP, Celio MR, Bloom FE, Rende M (1993) Presumptive Renshaw cells contain decreased calbindin during recovery from sciatic nerve lesions. Proc Natl Acad Sci USA 90:3048–3052.
Sassoe-Pognetto M, Fritschy JM (2000) Mini-review: gephyrin, a major postsynaptic protein of GABAergic synapses. Eur J Neurosci 12:2205–1220.
Schiavo G, Benfenati F, Poulain B, Rossetto O, Polverini de Laureto B, DasGupta BR, Montecucco C (1992) Tetanus and botulinum B neurotoxins block neurotransmitter release by proteolytic cleavage of synaptobrevin. Nature 359:832–835.
Schiavo G, Rossetto O, Catsicas S, Polverino de Laureto P, DasGupta BR, Benfenati F, Montecucco C (1993) Identification of the nerve terminal targets of botulinum neurotoxin serotypes A, D, and E. J Biol Chem 268:23784–23787.
Schwab ME, Thoenen H (1976) Electron microscopic evidence for a transsynaptic migration of tetanus toxin in spinal cord motoneurons: an autoradiographic and morphometric study. Brain Res 105:213–227.
Seil FJ, Drake-Baumann R (2000) TrkB receptor ligands promote activity-dependent inhibitory synaptogenesis. J Neurosci 20:5367–5373.
Takano K, Kano M (1973) Gamma-bias of the muscle poisoned by tetanus toxin. Naunyn Schmiedebergs Arch Pharmacol 276:413–420.
Takumi Y, Ramirez-Leon V, Laake P, Rinvik E, Ottersen OP (1999) Different modes of expression of AMPA and NMDA receptors in hippocampal synapses. Nat Neurosci 2:618–624.
Triller A, Cluzeaud F, Pfeiffer F, Betz H, Korn H (1985) Distribution of glycine receptors at central synapses: an immunoelectron microscopy study. J Cell Biol 101:683–688.
Turrigiano GG, Nelson SB (2004) Homeostatic plasticity in the developing nervous system. Nat Rev Neurosci 5:97–107.
van Keulen L (1981) Autogenic recurrent inhibition of individual spinal motoneurones of the cat. Neurosci Lett 21:297–300.
Van Zundert B, Alvarez FJ, Tapia JC, Yeh HH, Diaz E, Aguayo LG (2004) Developmental-dependent action of microtubule depolymerization on the function and structure of synaptic glycine receptor clusters in spinal neurons. J Neurophysiol 91:1036–1049.
Wiegand H, Wellhöner HH (1974) Type A botulinum toxin in cats: neural ascent and action on spinal cord reflexes. Naunyn Schmiedebergs Arch Pharmacol [Suppl] 282:R106.